Novel two-dimensional boron oxynitride predicted using USPEX evolutionary algorithm

Zakhar I. Popov,[1] Kseniya A. Tikhomirova,[1,2] Victor A. Demin,[1] Suman Chowdhury,[2] Artem R. Oganov,[2] Alexander G. Kvashnin,[2] and Dmitry G. Kvashnin[1,3]

[1] *Emanuel Institute of Biochemical Physics RAS, 4 Kosygin Street, Moscow 119334, Russian Federation*
[2] *Skolkovo Institute of Science and Technology, Skolkovo Innovation Center, 3 Nobel Street, Moscow 121025, Russian Federation*
[3] *Moscow Institute of Physics and Technology, Institutsky lane, Dolgoprudny 141701, Moscow Region, Russian Federation*

Contents

Stability of boron oxynitride $B_5N_3O_2$ S2
Electronic, mechanical, and optical properties S4
References S7

Stability of boron oxynitride $B_5N_3O_2$

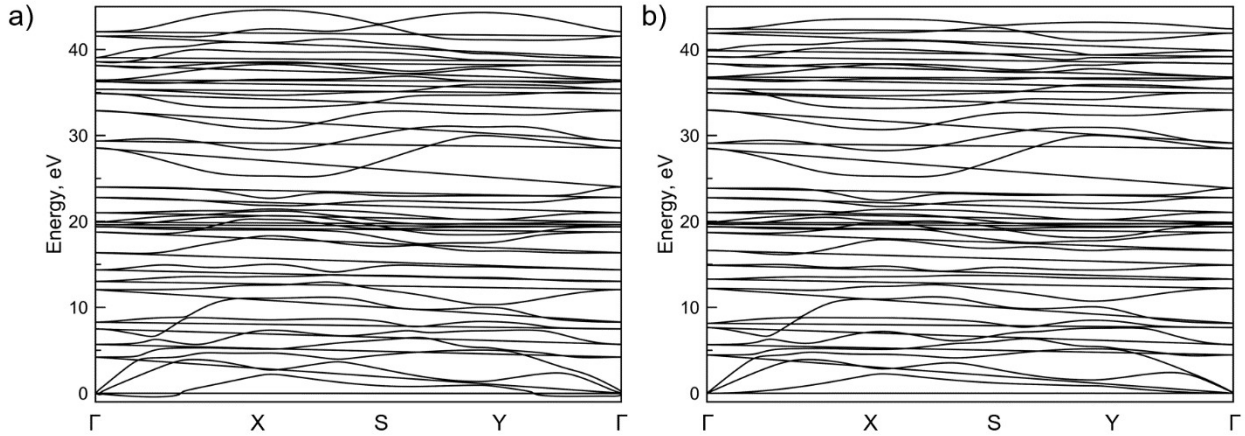

Fig. S1. Phonon dispersion of the $B_5N_3O_2$ monolayer calculated using the finite displacement method with (a) 3×3×1 supercell and (b) imposing both translational and rotational invariance.

Crystal symmetry, translational and rotational[1] invariances play an important role in describing the vibrational properties of any 2D system.[2] Because of the lack of consideration of these invariances in computations (e.g., when using a relatively small supercell in the frozen phonon method), the flexural acoustic phonon mode (i.e., the out-of-plane ZA mode) often shows linear dependence in the vicinity of the Γ-point.[3,4] This can sometimes significantly influence the phonon transport.[2,5] Many recent ab initio theories predict linear dependence of all three acoustic branches in different 2D materials like silicene,[6–8] phosphorene,[9] MoS_2,[10] WS_2,[11] MgB_6,[12] and WSe_2.[13] Other studies involving both ab initio and empirical calculations have proved that one of the acoustic modes must be quadratic in the long wavelength limit.[14–17] Accurate calculations have shown that the flexural acoustic mode must be quadratic near the center of the Brillouin zone.[2]

The phonon band structures without and with the imposed rotational invariance are shown in Fig. S1. Without the rotational invariance, the ZA phonon mode shows imaginary frequencies (Fig. S1a). However, after employing the rotational invariance, it becomes all real and exhibits a clear quadratic nature near the Γ-point of the Brillouin zone. We plotted the phonon band structures using PHONOPY[18] software which can only impose the translational invariance. To impose the rotational invariance,[1] we used hiPhive[19] software package which can employ both translational and rotational invariances on the force constants that we obtained using PHONOPY package.

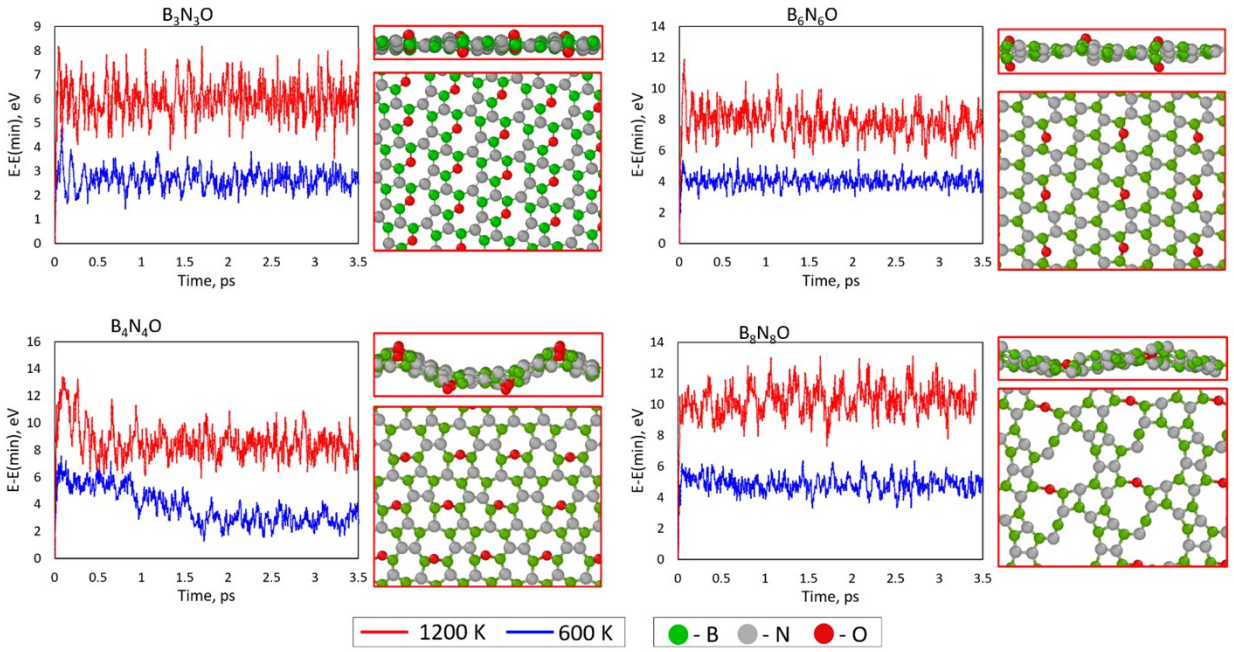

Fig. S2. AIMD simulations of the B–N–O structures with various oxygen concentrations at 600 K (blue line) and 1200 K (red line). The side and top views of the atomic structures at 3 ps and 1200 K are presented in the right panels for each composition. The boron, nitrogen, and oxygen atoms are shown in green, gray, and red, respectively.

Electronic, mechanical, and optical properties

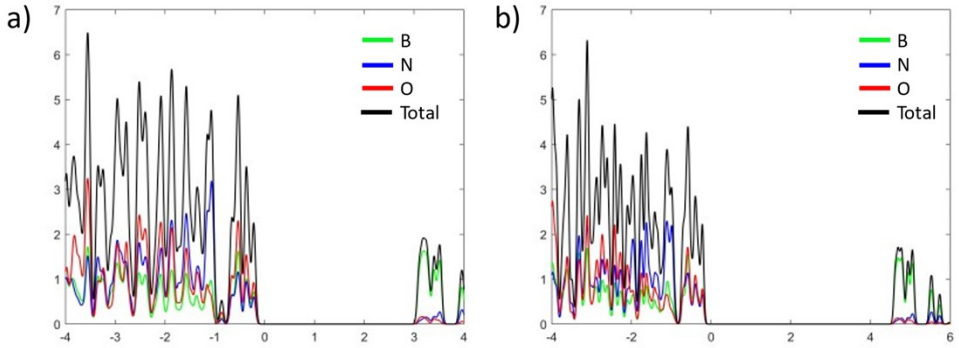

Fig. S3. Density of electronic states of $B_5N_3O_2$, calculated using: a) the PBE functional [28] and b) the hybrid functional of Heyd, Scuseria, and Ernzerhof (HSE06) [20].

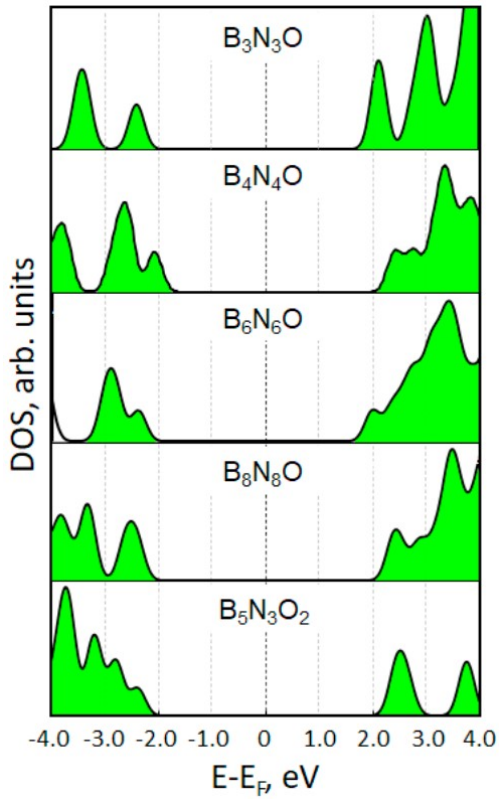

Fig. S4. Density of electronic states, calculated using the hybrid functional of Heyd, Scuseria, and Ernzerhof (HSE06) [20], of the B–N–O compositions with unique atomic structures.

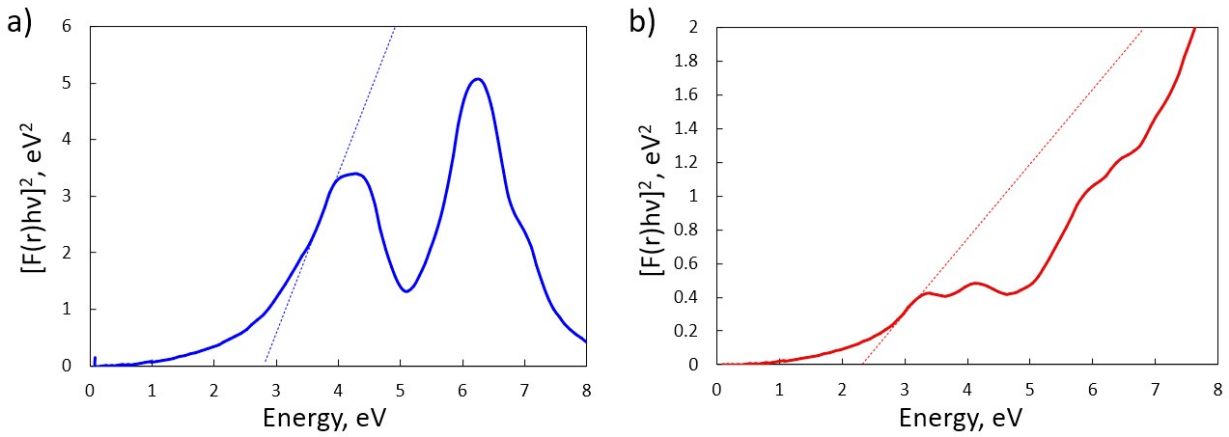

Fig. S5 Kubelka–Munk plots of $B_5N_3O_2$ structure calculated using PBE functional [28] for longitudinal (a) and transverse (b) direction. By dotted line the linear extrapolation presented.

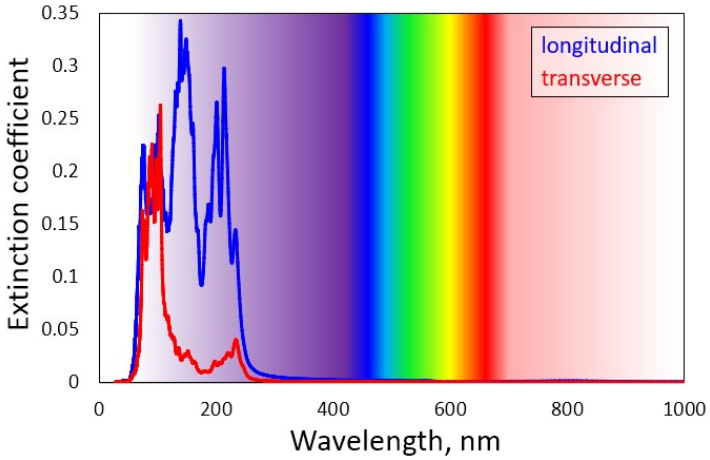

Fig. S6 Wavelength dependence of the extinction coefficient of $B_5N_3O_2$ monolayer calculated using the hybrid functional of Heyd, Scuseria, and Ernzerhof (HSE06) [20]. Bule and red curves correspond to the longitudinal and transverse directions, respectively.

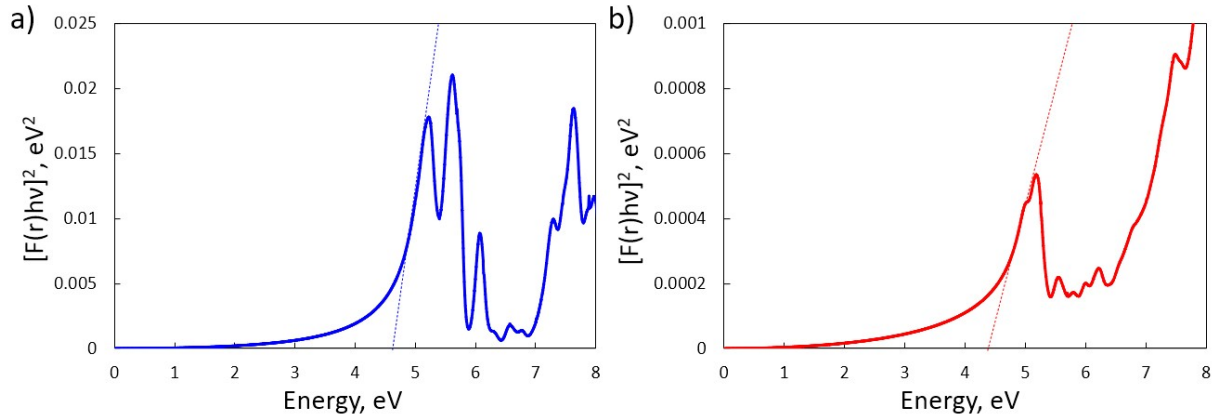

Fig. S7 Kubelka–Munk plots of $B_5N_3O_2$ structure calculated using the hybrid functional of Heyd, Scuseria, and Ernzerhof (HSE06) [20] for longitudinal (a) and transverse (b) direction. By dotted line the linear extrapolation presented.

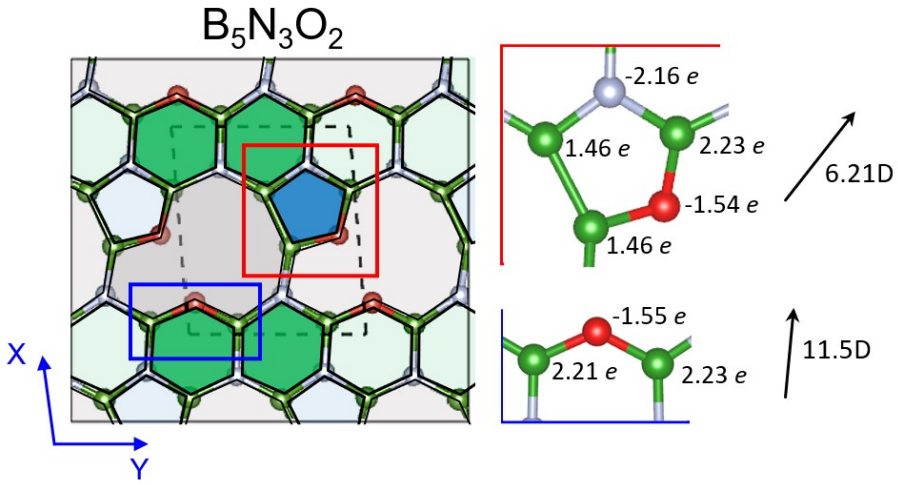

Fig. S8. Bader charge analysis and the local dipole moments of the individual components of $B_5N_3O_2$ structure.

Table S1. Piezoelectric tensor e_{ij} (C/m^2) of the B–N–O structures

$B_5N_3O_2$					
1.15	0.07	0.08	2.14	-0.07	0.24
2.28	-1.05	-0.02	0.03	-0.20	-0.21
-0.04	-0.18	-0.03	-0.03	-0.02	0.03
B_8N_8O					
0.14	1.75	0.33	0.79	-0.04	-0.48
-0.60	0.78	0.11	0.81	-0.09	-0.01
0.16	1.06	0.16	0.63	-0.18	-0.25
B_6N_6O					
-1.45	0.25	0.00	-0.04	-0.01	-0.59
-0.06	0.04	0.00	1.79	0.76	-0.02
-0.12	0.20	0.09	0.00	0.00	0.03
B_4N_4O					
0.04	0.28	0.04	1.47	-0.06	-1.02
-0.70	-1.66	0.02	0.05	0.71	-0.01
-0.16	0.22	-0.07	0.04	0.05	0.01
B_4N_3O					
0.01	-0.01	0.02	0.04	0.01	1.70
-1.75	5.31	0.62	-0.01	0.11	0.00
0.27	0.27	0.10	0.00	0.02	0.00
B_3N_3O					
2.46	-1.91	-0.01	0.40	0.01	-0.01
-0.46	1.34	0.07	-1.88	-0.01	0.01
-0.01	-0.01	0.00	0.00	0.00	0.00

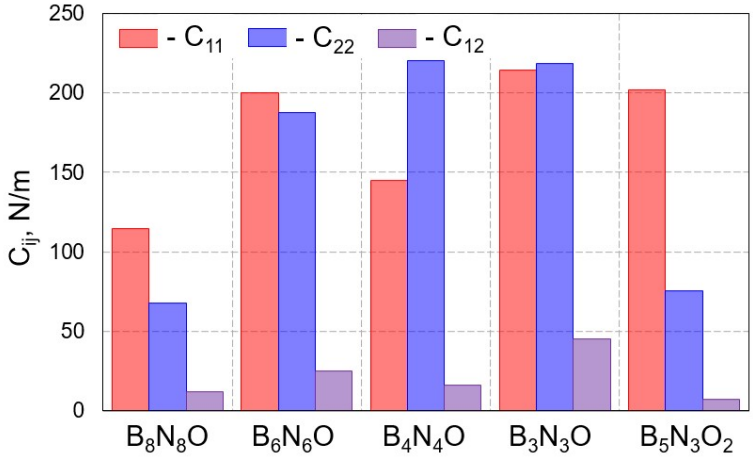

Fig. S9. Calculated values of the elastic constants of the predicted B–N–O structures with different oxygen concentration.

REFERENCES

1 M. Born and K. Huang, *American Journal of Physics*, 1955, **23**, 474–474.

2 J. Carrete, W. Li, L. Lindsay, D. A. Broido, L. J. Gallego and N. Mingo, *Materials Research Letters*, 2016, **4**, 204–211.

3 Y. D. Kuang, L. Lindsay, S. Q. Shi and G. P. Zheng, *Nanoscale*, 2016, **8**, 3760–3767.

4 A. S. Nissimagoudar, A. Manjanath and A. K. Singh, *Phys. Chem. Chem. Phys.*, 2016, **18**, 14257–14263.
5 B. Peng, H. Zhang, H. Shao, Y. Xu, G. Ni, R. Zhang and H. Zhu, *Phys. Rev. B*, 2016, **94**, 245420.
6 A. Manjanath, V. Kumar and A. K. Singh, *Phys. Chem. Chem. Phys.*, 2013, **16**, 1667–1671.
7 H. Xie, M. Hu and H. Bao, *Appl. Phys. Lett.*, 2014, **104**, 131906.
8 X. Gu and R. Yang, *Journal of Applied Physics*, 2015, **117**, 025102.
9 A. Jain and A. J. H. McGaughey, *Scientific Reports*, 2015, **5**, 8501.
10 X. Fan, W. T. Zheng, J.-L. Kuo and D. J. Singh, *J. Phys.: Condens. Matter*, 2015, **27**, 105401.
11 A. Berkdemir, H. R. Gutiérrez, A. R. Botello-Méndez, N. Perea-López, A. L. Elías, C.-I. Chia, B. Wang, V. H. Crespi, F. López-Urías, J.-C. Charlier, H. Terrones and M. Terrones, *Scientific Reports*, 2013, **3**, 1755.
12 S.-Y. Xie, X.-B. Li, W. Q. Tian, N.-K. Chen, Y. Wang, S. Zhang and H.-B. Sun, *Phys. Chem. Chem. Phys.*, 2014, **17**, 1093–1098.
13 W.-X. Zhou and K.-Q. Chen, *Scientific Reports*, 2015, **5**, 15070.
14 X. Zhang, H. Xie, M. Hu, H. Bao, S. Yue, G. Qin and G. Su, *Phys. Rev. B*, 2014, **89**, 054310.
15 G. Qin, Q.-B. Yan, Z. Qin, S.-Y. Yue, M. Hu and G. Su, *Phys. Chem. Chem. Phys.*, 2015, **17**, 4854–4858.
16 L. Zhu, G. Zhang and B. Li, *Phys. Rev. B*, 2014, **90**, 214302.
17 A. Molina-Sánchez and L. Wirtz, *Phys. Rev. B*, 2011, **84**, 155413.
18 A. Togo, F. Oba and I. Tanaka, *Phys. Rev. B*, 2008, **78**, 134106.
19 F. Eriksson, E. Fransson and P. Erhart, *Advanced Theory and Simulations*, 2019, **2**, 1800184.
20 A. V. Krukau, O. A. Vydrov, A. F. Izmaylov and G. E. Scuseria, *The Journal of Chemical Physics*, 2006, **125**, 224106.